Magnetoresistance and Shubnikov–de Haas oscillations in layered Nb_3SiTe_6 thin flakes

Linlin An,[1,2] Hongwei Zhang,[1,2] Jin Hu,[3] Xiangde Zhu,[1] Wenshuai Gao,[1,2] Jinglei Zhang,[1] Chuanying Xi,[1] Wei Ning,[1,*] Zhiqiang Mao,[4] and Mingliang Tian[1,5,6,†]

[1]*Anhui Province Key Laboratory of Condensed Matter Physics at Extreme Conditions, High Magnetic Field Laboratory, Chinese Academy of Sciences, Hefei 230031, Anhui, China*

[2]*Department of physics, University of Science and Technology of China, Hefei 230026, China*

[3]*Department of Physics, Institute for Nanoscience and Engineering, University of Arkansas, Fayetteville, Arkansas 72701, USA*

[4]*Department of Physics and Engineering Physics, Tulane University, New Orleans, Louisiana 70118, USA*

[5]*School of Physics and Materials Science, Anhui University, Heifei 230601, China*

[6]*Collaborative Innovation Center of Advanced Microstructures, Nanjing University, Nanjing 210093, China*

(Received 15 March 2018; published 19 June 2018)

We present the magnetoresistance (MR) and Hall resistivity of layered ternary Nb_3SiTe_6 thin flakes with magnetic field up to 33 T. The flakes show strong angle-dependent MR properties and unsaturated quasilinear dependence accompanied with Shubnikov–de Haas (SdH) oscillations. Hall resistivity study demonstrates that the hole carriers dominate the transport properties in the whole temperature range. The angle-dependent SdH oscillations reveal a two-dimensional Fermi surface of Nb_3SiTe_6. Furthermore, by analysis of SdH oscillations, we observed a nontrivial π-Berry phase in the SdH oscillations which suggests the nontrivial topological nature of Nb_3SiTe_6.

DOI: 10.1103/PhysRevB.97.235133

Research on two-dimensional (2D) atomic crystals is one of the leading topics in condensed-matter physics and materials science [1,2]. The excellent properties in 2D materials, such as the high carrier mobility in graphene [3,4] and the large direct band gaps in transition-metal dichalcogenides MoS_2 monolayers [5,6], have attracted significant interest for their fascinating electrical, optical, and mechanical properties. Recently, ternary telluride compound Nb_3SiTe_6 has attracted attention. This material has similar layered crystal structure with MoS_2 and can be thinned down to one-unit-cell-thick 2D sheets using microexfoliation technique [7]. It was found that a few-layer Nb_3SiTe_6 crystal shows unusual quantum transport properties compared with its bulk crystals. Especially, an unexpected enhancement of weak antilocalization signature was observed in magnetotransport when the thickness is reduced below a few unit cells thickness, indicating the theoretically predicted suppression of electron-phonon interaction caused by the crossover of phonon spectrum from 3D to 2D. However, the detailed electronic structures including the information of Fermi surface in layered Nb_3SiTe_6 is still lacking. Moreover, a recent theory work [8] suggested that Nb_3SiTe_6 bulk crystal possess accidental Dirac loops and essential fourfold nodal lines [9,10] in the absence of spin-orbit coupling (SOC), and an hourglass Dirac loop [11,12] in the presence of SOC. There is also no evidence of topological properties provided by the Shubnikov–de Haas (SdH) quantum oscillations from the transport measurement.

Here we present systematically magnetotransport studies of Nb_3SiTe_6 thin flakes exfoliated from bulk crystals, including angle-dependent magnetoresistance (MR) and Hall resistivity measurements. We found that the MR exhibits unsaturated quasilinear behavior with magnetic fields up to 33 T, accompanied by the SdH quantum oscillations. Hall resistance results suggest that the hole-type carriers dominate the transport properties in the whole temperature range. By analysis of the SdH oscillations, we observed a nontrivial π-Berry phase in the SdH oscillations. The angular dependence of the oscillation reveals a 2D nature of the Fermi surface in Nb_3SiTe_6. All these transport results provide important information on the electronic structures and the nontrivial topological nature of Nb_3SiTe_6.

The crystal structure of Nb_3SiTe_6 is formed from the stacks of sandwich layers which is similar to that of MoS_2, as shown in the inset of Fig. 1(a). In MoS_2, each S-Mo-S sandwich layer is composed of edge-sharing trigonal MoS_6 prisms [13], whereas the Te-(Nb,Si)-Te sandwich layer of Nb_3SiTe_6 consists of face and edge-sharing $NbTe_6$ prisms and Si ions insert into the interstitial sites among these prisms. The micaceous nature of Nb_3SiTe_6 allows it to be thinned down to atomically thin 2D crystals by microexfoliation [14]. The Nb_3SiTe_6 single crystals used in this work were grown via chemical vapor transport [7]. Here, the Nb_3SiTe_6 thin flakes with different thickness were obtained by mechanically exfoliating the bulk crystal, followed by directly transferring onto Si/SiO_2 substrate. Hall-bar devices were fabricated by standard electron-beam lithography followed by a Au (80 nm)/Ti (10 nm) evaporation and lift-off process. An image of a Hall bar device is shown in the lower inset of Fig. 1(b). Transport measurements were performed with a physical properties measurement system and the 35-T dc-resistive magnet at the High Magnetic Field Laboratory in Hefei, China.

*ningwei@hmfl.ac.cn
†tianml@hmfl.ac.cn

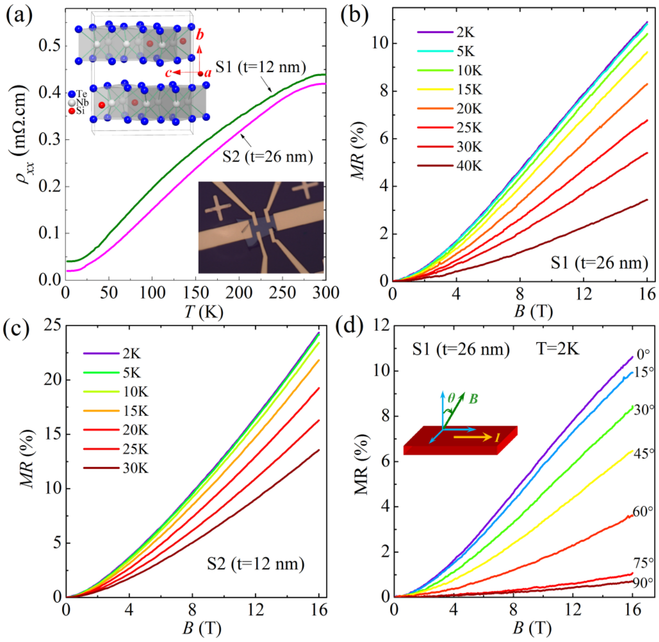

FIG. 1. (a) Longitudinal resistivity of Nb_3SiTe_6 single crystal in zero magnetic field for sample S1 (26 nm) and sample S2 (12 nm) from 2 to 300 K. The upper inset shows the crystal structure of Nb_3SiTe_6. The lower inset shows the scanning electron microscope image of a Hall bar device used in the measurement process. (b), (c) The MR with magnetic field applied perpendicular to the thin flake at various temperatures for sample S1 ($t = 26$ nm) and S2 ($t = 12$ nm), respectively. (d) Angle-dependent MR at 2 K for sample S1 ($t = 26$ nm).

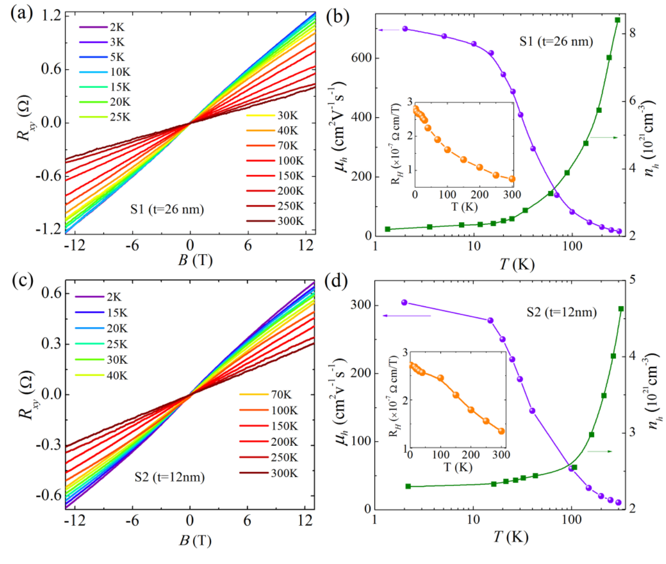

FIG. 2. (a), (c) Respectively, the Hall resistance R_{xy} of sample S1 ($t = 26$ nm) and S2 ($t = 12$ nm) as a function of magnetic field at various temperatures. (b), (d) Respectively, the temperature dependence of the mobility and the carrier density. The insets show the temperature dependence of the Hall coefficient R_H.

Figure 1(a) shows the temperature dependence of the longitudinal resistivity ρ_{xx} at zero magnetic field for two samples S1 and S2 with thickness of $t = 26$ nm and $t = 12$ nm, respectively. The temperature dependence of the resistivity shows a metallic behavior, which is similar to the bulk crystals [7]. Figures 1(b) and 1(c) show magnetoresistance of sample S1 ($t = 26$ nm) and S2 ($t = 12$ nm) with magnetic field applied perpendicular to the flake at different temperatures, respectively. The MR shows a semiclassical quadratic field dependence in low-field range, while it becomes quasilinear in high-field range for both samples. It can be noted that the MR in sample S2 ($\sim$24% at 16 T and 2 K) is larger than that in thicker sample S1 ($\sim$11% at 16 T and 2 K). The unusual larger MR in thinner sample might be attributed to the reduction of electron-phone interaction [7]. Furthermore, no weak antilocalization effect was observed in our transport measurements. This might be due to the fact that these samples are not thin enough. Figure 1(d) shows the angle-dependent MR by tilting the magnetic field from b-axis direction ($\theta = 0^\circ$) to parallel to the applied current ($\theta = 90^\circ$) in the (a, b) plane. The MR decreases dramatically from 8.5% at $\theta = 0^\circ$ to 0.55% at $\theta = 90^\circ$ under $B = 16$ T, indicating a significant anisotropic MR with amplitude ratio up to 15. Such large angle-dependent MR behavior suggests potential applications in electric devices.

To further investigate the transport properties of Nb_3SiTe_6, we systemically measured the Hall resistivity at different temperatures. The Hall resistance R_{xy} as a function of magnetic fields for various temperatures of sample S1 (26 nm) and S2 (12 nm) is presented in Figs. 2(a) and 2(c), respectively. For two samples, the Hall resistance R_{xy} shows linear dependence with the applied magnetic fields and the Hall coefficient R_H extracted from $R_H \propto R_{xy}/B$, as shown in the inset of Figs. 2(b) and 2(d), remains positive in the whole measured temperature range, indicating that the hole carriers are dominated in the transport properties. Since the Hall resistance exhibits a linear behavior, we can evaluate the carrier density by the formula $n = 1/R_H e$ and the mobility μ by the relationship $\mu = R_H/\rho_{xx}$, where e, σ, and n are the electron charge, zero field conductivity, and carrier density, respectively. The obtained results are shown in Figs. 2(b) and 2(d) for samples S1 and S2, respectively. With temperature decreasing, the hole density n_h of both flakes S1 and S2 decreases monotonically from 8.4 $\times 10^{21}$ cm^{-3} and 4.3 $\times 10^{21}$ cm^{-3} at 300 K to 2.2 $\times 10^{21}$ cm^{-3} and 2.3 $\times 10^{21}$ cm^{-3} at 2 K, while the corresponding mobility μ_h increases gradually from 16.9 cm^2 V^{-1}s^{-1} and 10.3 cm^2 V^{-1}s^{-1} at 300 K to 699.9 cm^2 V^{-1}s^{-1} and 304 cm^2 V^{-1}s^{-1} at 2 K, respectively. Thus it can be found that during the reduction of sample thickness from 26 to 12 nm, the carrier mobility decreases while the density stays unchanged.

As shown in Fig. 1, the MR shows no saturation with magnetic field up to 16 T. To verify such an unsaturated MR being validated at even higher fields, we have performed MR measurements using a dc-resistive magnet. Figure 3(a) presents the angle-dependent MR for sample S2 ($t = 12$ nm), in which the R_{xx} shows no saturation with fields up to 33 T. Above 20 T, resistance oscillations superimposed on the MR curves can be resolved. After subtracting a three-order polynomial background, the relative oscillatory component ΔR_{xx} versus $1/B\cos\theta$ was displayed in Fig. 3(b) at different angles. As expected from the successive emptying of the Landau levels

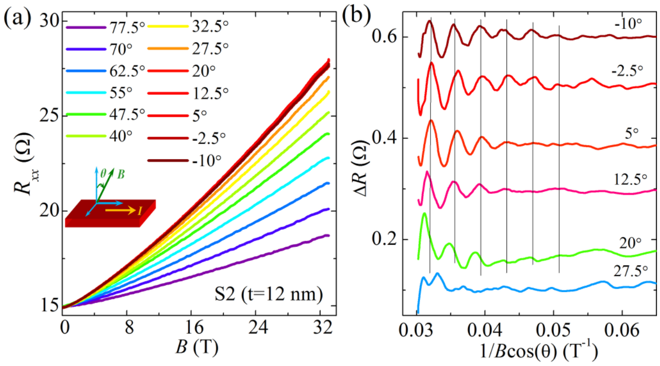

FIG. 3. (a) The longitudinal resistance R_{xx} of sample S2 ($t = 12$ nm) as a function of magnetic field under different field orientation angles θ. (b) The oscillatory component ΔR_{xx}, extracted from R_{xx} by subtracting a smooth background, as a function of $1/B\cos(\theta)$ at various angles.

when the magnetic field is increased, ΔR_{xx} is periodic with $1/B\cos\theta$. Above $\theta = 20^\circ$, the oscillation is too weak to be identified clearly. Below $\theta = 20^\circ$, all the maximum (or minimum) of these oscillations appear at the same $B_\perp = B\cos\theta$ for all angles, providing evidence of a quasi-2D character of the electronic state [15–18].

In order to obtain more information about the electronic structure, we have investigated the temperature-dependent MR under high magnetic fields, as shown in Fig. 4(a). Figure 4(b) shows the relative oscillatory component ΔR_{xx} versus $1/B$ at different temperatures for sample S2 ($t = 12$ nm). As shown in the inset of Fig. 4(a), a single oscillation frequency $F = 263$ T is identified from fast Fourier transform (FFT) analysis of these data. Thus we get the cross-sectional area of the Fermi surface A_F is 0.025 Å^{-2} by using Onsager relation: $F = (\hbar/2\pi e)A_F$ [19], where A_F is the cross-sectional area of the Fermi surface. The corresponding wave vector k_F is 0.0895 Å. To estimate the cyclotron mass, we have fitted the temperature-dependent FFT amplitude by the Lifshitz-Kosevich (LK) formula [20].

$$\Delta R_{xx}(T,B)/\Delta R_{xx}(B=0) \propto \frac{2\pi^2 k_B T m^*/eB}{\sinh\left(\frac{2\pi^2 k_B T m^*}{eB}\right)}, \qquad (1)$$

where k_B is Boltzmann constant and m^* is cyclotron mass. By taking the oscillation amplitude of the peak $B = 31$ T, the effective mass of the carriers m^* is extracted to be 1.2 m_0 by performing a theoretical fit with the above equation [Fig. 4(c)]. Thus the Fermi velocity v_F is 9.3×10^4 m/s calculated by $v_F = \hbar k_F/m^*$, and the Fermi energy $E_F = m^* v_F^2 = 54.89$ meV. The Dingle temperature $T_D = \hbar/2\pi k_B \tau_Q$, which is related to the quantum-scattering lifetime τ_Q is obtained to be about 6.4 K based on Eq. (1) from the field-dependent amplitudes of the quantum oscillations at fixed temperatures as shown in the inset of Fig. 4(c). Hence, the corresponding quantum-scattering lifetime is calculated to be $\tau_Q = 1.9 \times 10^{-13} s$ and the quantum mobility estimated by $\mu_Q = \frac{e\tau_Q}{m^*}$ is 279.9 cm^{2}V^{-1}s^{-1}, which is consistent with the mobility estimated from the Hall data.

Recent theory work [8] suggests that Nb_3SiTe_6 host accidental Dirac loops and essential fourfold nodal lines in the

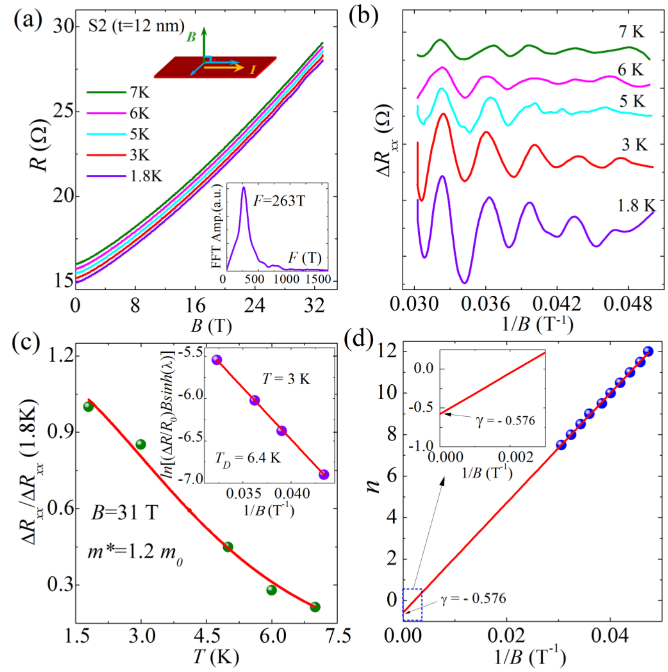

FIG. 4. (a) Longitudinal magnetoresistance of sample S2 ($t = 12$ nm) at different temperatures with a maximum field of 33 T. The curves are shifted for clarity. (b) The oscillatory component ΔR_{xx} as a function of $1/B$ at various temperatures. (c) Temperature dependence of the scaled oscillation amplitude at $B = 31$ T. The solid curves are the fits to the Lifshitz-Kosevich formula from 1.8 to 7 K. The inset shows the Dingle plot of the SdH oscillations at $T = 3$ K. (d) Landau-level index n extracted from SdH oscillations plotted as function of the $1/B$.

absence of spin-orbit coupling, and an hourglass Dirac loop emerges in the presence of SOC. To seek the possible evidence for relativistic fermions in Nb_3SiTe_6, we examined the Berry phase accumulated along cyclotron orbits. For a Dirac material, pseudospin rotation under a magnetic field should result in a nontrivial Berry phase, which can be accessed from the Landau-level (LL) index fan diagram or the direct fit of the SdH oscillation pattern to the LK formula. For a 2D or quasi-2D system with relativistic fermions, the intercept on the n_0 axis of the LL fan diagram is expected to be 1/2, for which the corresponding Berry phase is $2\pi n_0 = c\pi$ [21]. In Fig. 4(d), we have plotted the Landau index n as function of the $1/B$. Here the ΔR_{xx} peak positions in $1/B$ were assigned to be integer indices and the ΔR_{xx} valley positions were assigned to half-integer indices [22]. All the points almost fall on a straight line, and the linear fitting gives an intercept −0.57(6), close to the expected value of 0.5 for a 2D or quasi-2D system with relativistic fermions [23].

In summary, we have performed magnetotransport study on Nb_3SiTe_6 thin flakes under high magnetic fields up to 33 T. The MR shows unsaturated quasilinear behavior accompanied with SdH oscillations. The Hall resistance suggests that hole-type carriers dominate the transport properties. The angle-dependent SdH oscillations reveal a 2D character of the Fermi surface of Nb_3SiTe_6. We extracted a nontrivial π-Berry phase in the SdH oscillations which is consistent with the recent theory and suggest the nontrivial topological nature of Nb_3SiTe_6.

This work was supported by the National Key Research and Development Program of China Grant No. 2016YFA0401003; the Natural Science Foundation of China (Grants No. 11774353, No. 11574320, No. 11374302, No. U1432251, and No. U1732274); The International Users of Hefei Science Center of CAS (Grant No. 2016HSC-IU009); and the CAS/SAFEA international partnership program for creative research teams of China.

L.A. and H.Z. contributed equally to this work.

[1] A. K. Geim and I. V. Grigorieva. Nature (London) **499**, 419 (2013).

[2] M. Chhowalla, H. S. Shin, G. Eda, L.-J. Li, K. P. Loh, and H. Zhang, Nat. Chem. **5**, 263 (2013).

[3] K. S. Novoselov *et al.*, Science **306**, 666 (2004).

[4] Y. B. Zhang, Y. W. Tan, H. L. Stormer, and P. Kim, Nature (London) **438**, 201 (2005).

[5] K. F. Mak, C. Lee, J. Hone, J. Shan, and T. F. Heinz. Phys. Rev. Lett. **105**, 136805 (2010).

[6] H. Zeng, J. Dai, W. Yao, D. Xiao, and X. Cui, Nat. Nanotechnol. **7**, 490 (2012).

[7] J. Hu, X. Liu, C. L. Yue, J. Y. Liu, H. W. Zhu, J. B. He, J. Wei, Z. Q. Mao, L. Yu. Antipina, Z. I. Popov *et al.*, Nat. Phys. **11**, 471 (2015).

[8] S. Li, Y. Liu, S.-S. Wang, Z.-M. Yu, S. Guan, X.-L. Sheng, Y. Yao, and S. A. Yang, Phys. Rev. B **97**, 045131 (2018).

[9] H. Weng, Y. Liang, Q. Xu, R. Yu, Z. Fang, X. Dai, and Y. Kawazoe, Phys. Rev. B **92**, 045108 (2015).

[10] S. A. Yang, H. Pan, and F. Zhang, Phys. Rev. Lett. **113**, 046401 (2014).

[11] Z. Wang, A. Alexandradinata, R. J. Cava, and B. A. Bernevig, Nature (London) **532**, 189 (2016).

[12] J. Ma, C. Yi, B. Lv, Z. Wang, S. Nie, L. Wang, L. Kong, Y. Huang, P. Richard, P. Zhang *et al.*, Sci. Adv. **3**, e1602415 (2017).

[13] O. Lopez-Sanchez, D. Lembke, M. Kayci, A. Radenovic, and A. Kis, Nat. Nanotechnol. **8**, 497 (2013).

[14] J. Li, M. E. Badding, and F. DiSalvo, J. Inorg. Chem. **31**, 1050 (1992).

[15] J. G. Analytis, R. D. McDonald, S. C. Riggs, J.-H. Chu, G. S. Boebinger and I. R. Fisher, Nat. Phys. **6**, 960 (2010)

[16] W. Ning, F. Y. Kong, C. Y. Xi, D. Graf, H. F. Du, Y. Han, J. Y. Yang, M. L. Tian, and Y. H. Zhang, ACS Nano **8**, 7506 (2014)

[17] K. F. Wang, D. Graf, H. C. Lei, S. W. Tozer, and C. Petrovic, Phys. Rev. B **84**, 220401(R) (2011).

[18] N. Kumar, C. Shekhar, S.-C. Wu, I. Leermakers, U. Zeitler, B. H. Yan, and C. Felser, Phys. Rev. B **93**, 241106 (2016).

[19] D. Shoenberg, *Magnetic Oscillations in Metals* (Cambridge University Press, Cambridge, England, 1984).

[20] H. Murakawa, M. S. Bahramy, M. Tokunaga, Y. Kohama, C. Bell, Y. Kaneko, N. Nagaosa, H. Y. Hwang, and Y. Tokura, Science **342**, 1490 (2013).

[21] J. Y. Liu, J. Hu, Q. Zhang, D. Graf, H. B. Cao, S. M. A. Radmanesh, D. J. Adams, Y. L. Zhu, G. F. Cheng, X. Liu *et al.*, Nat. Mater. **16**, 905 (2017)

[22] Y. Ando *et al.*, J. Phys. Soc. Jpn. **82**, 102001 (2013).

[23] D. Xiao, M.-C. Chang, and Q. Niu, Rev. Mod. Phys. **82**, 1959 (2010).